Manuscript

Characterization of iGABASnFR2 for in vivo mesoscale imaging of intracortical GABA dynamics

Authors: Edris Rezaei*[1],Setare Tohidi[1], Mojtaba Nazari-Ahangarkolaee[1],Javad Karimi Abadchi[2], Nicholas J. Michelson[3], Timothy H. Murphy [3]

[1]Canadian Centre for Behavioural Neuroscience, University of Lethbridge; Lethbridge, AB, Canada

[2]Department of Psychiatry, the Douglas Research Centre, McGill University, Montréal, QC, Canada

[3]Department of Psychiatry, Djavad Mowafaghian Centre for Brain Health, University of British Columbia, Vancouver, BC, Canada

*** Corresponding author**:

Edris Rezaei (edris.rezaei@uleth.ca)

Address:

Edris Rezaei, Department of Neuroscience, University of Lethbridge, 4401 University Dr W, Lethbridge, AB T1K 3M4, Canada

Abstract

Most genetically encoded sensors for mesoscopic cortical imaging target excitatory signals, leaving inhibitory dynamics less understood. Capturing large-scale extracellular GABA activity in vivo is essential for understanding how inhibition shapes cortical processing across brain states. To validate the genetically encoded sensor iGABASnFR2 for mesoscale in vivo imaging of extracellular GABA dynamics and to assess how inhibitory activity reorganizes with sensory input, behavioral state, and pharmacological manipulation. We used wide-field imaging in head-fixed mice expressing iGABASnFR2 via retro-orbital AAV injection. Imaging was performed under anesthesia, during quiet wakefulness, natural sleep (NREM, REM), and after administration of the GABA reuptake inhibitor Tiagabine. We analyzed sensory-evoked and spontaneous GABA signals using seed-pixel correlation and spectral analyses. iGABASnFR2 revealed delayed, modality-specific inhibitory responses to sensory stimulation that were stronger and faster in the contralateral cortex. These responses were conserved between anesthesia and quiet wakefulness. During spontaneous activity, GABAergic networks showed state-dependent reorganization: widespread bilateral synchrony was observed in NREM and wakefulness, while REM sleep showed reduced GABA levels and decoupling. Tiagabine elevated baseline GABA, prolonged sensory responses, and enhanced long-range inhibitory connectivity. iGABASnFR2 enables reliable, real-time imaging of extracellular GABA across large cortical areas. These findings demonstrate its utility for tracking state-dependent inhibitory motifs and highlight the dynamic architecture of cortical inhibition in health and disease.

Keywords: iGABASnFR2; GABA; wide-field imaging; inhibition; spontaneous activity.

Introduction

The nervous system consists of various specialized cell types, including neurons and glial cells; among these, neurons serve as the primary functional units responsible for transmitting and processing information throughout the brain and body. Neurons can be broadly categorized into excitatory and inhibitory types, which work together to regulate brain function. Excitatory neurons primarily release glutamate which is the major neurotransmitter in the nervous system to facilitate communication between neurons across different brain regions (Zhou & Danbolt, 2014), while inhibitory neurons mainly release gamma-aminobutyric acid (GABA) to stabilize neural networks by balancing excitatory activity and preventing excessive neuronal firing (Froemke, 2015). Maintaining this precise balance between excitation and inhibition is essential for sensory processing, memory formation, and motor control. (Tatti et al., 2017; Yuste, 2005). Through temporally and spatially precise modulation of neuronal activity, inhibitory signaling contributes to a wide range of brain functions, including sensory processing, circuit refinement, and the regulation of oscillatory dynamics (Markram et al., 2004; Tremblay et al., 2016; Kepecs & Fishell, 2014; Ferguson & Gao, 2018; Urban-Ciecko et al., 2016). Disruptions in GABAergic signaling underlie a variety of neurological and psychiatric disorders, including epilepsy, schizophrenia, and autism spectrum disorders, highlighting the clinical importance of understanding GABAergic modulation in both health and disease (De Lanerolle et al., 1989; Lewis & Moghaddam, 2006; Curley & Lewis, 2012; Marin, 2012; Rubenstein & Merzenich, 2003; Ben-Ari, 2006; Gonzalez-Burgos & Lewis, 2008). Despite the recognized significance of GABA, direct, real-time visualization of GABAergic signaling in vivo has remained challenging. Recent advancements in genetically encoded neurotransmitter sensors have profoundly improved the capacity to monitor neural dynamics at various spatial scales (Marvin et al., 2013). For instance, the glutamate sensor iGluSnFR enabled high-resolution, real-time imaging of excitatory neurotransmission, providing unprecedented insights into cortical connectivity and sensory-driven neural activity in awake and anesthetized animals (Marvin et al., 2018; Xie et al., 2016). Expanding upon recent technological advances, the genetically encoded fluorescent sensor iGABASnFR2 was recently developed to detect extracellular GABA dynamics with high specificity and sensitivity (Marvin et al., 2019). This sensor permits real-time, in vivo monitoring of extracellular GABA, providing a powerful tool for visualizing GABA's spatial and temporal dynamics across large-scale cortical regions.

Wide-field imaging with iGABASnFR2 enables comprehensive mapping of inhibitory circuits beyond traditional localized recordings. However, a detailed characterization of its functionality across different brain states, sensory modalities, and pharmacological conditions is still needed for a complete validation of its utility in neuroscience research, highlighting the need for further collaborative research in this area. In this study, we comprehensively characterized spontaneous and sensory-evoked GABAergic activity across the dorsal cortex using wide-field imaging of iGABASnFR2 sensor in natural sleep, awake mice, and under 1% isoflurane anesthesia. Additionally, we assess the effects of Tiagabine, a GABA reuptake inhibitor, to further characterize sensor performance and demonstrate its sensitivity to pharmacological manipulation of cortical GABA levels. These results not only validate the robustness and sensitivity of iGABASnFR2 as a practical tool for monitoring GABAergic neurotransmission in vivo but also lay a solid foundation for future studies into inhibitory dynamics in health and disease, including conditions like epilepsy, schizophrenia, and autism spectrum disorders.

Material and methods

Animal subjects

The University of Lethbridge animal care committee approved all procedures, which adhered to the guidelines set forth by the Canadian Council on Animal Care and Use. We used 20 young adult (6–8 weeks old) C57BL/6 mice (12 males and 8 females). Mice were accommodated in transparent plastic cages within a 12-hour light-dark cycle,with lights turning on at 7:30 AM and provided unrestricted food and water access. Room temperature was maintained at 24 ± 2 °C, and relative humidity was kept between 40% and 50%.

Viral constructs

The viral constructs originated from the Viral Vector Core of the Canadian Neurophotonics Platform (RRID: SCR_016477). The AAV2/PHP.N-CAG-iGABASnFR2 and AAV2/PHP.N-CAG-csGFP, obtained from Addgene and subcloned by the CNP Viral Vector Core, underwent purification, resulting in a concentration of 1.5 x 10^{13} genome copies per milliliter (GC mL-1).

102 **Retro-orbital injection**

103 For retro-orbital viral injections (Yardeni et al., 2011), mice aged 4 to 6 weeks were used. The
104 average body weight was approximately 22 g for males and 18 g for females at the time of
105 injection. mice were anesthetized with 3% isoflurane and maintained at 2–2.5% during the
106 procedure. Analgesia was provided by subcutaneous Metacam (5 mg/kg), and body temperature
107 was regulated using a heating blanket. After confirming sufficient anesthetic depth, topical
108 anesthesia (0.5% proparacaine hydrochloride) was applied to the eye. Gentle pressure induced
109 mild eye protrusion, and a 30-gauge needle was inserted through the medial canthus at a 30° angle
110 into the retro-orbital space. Mice received 1.4×10^{11} genome copies (GC) of either AAV2/PHP.N-
111 CAG-iGABASnFR2 or AAV2/PHP.N-CAG-csGFP, using the PHP.N capsid for widespread CNS
112 expression, as originally described by (Chan et al. 2017).

113 **Drug Administration**

114 Tiagabine hydrochloride (Cat #SML0035, Sigma-Aldrich Canada) was purchased from Sigma-
115 Aldrich. Tiagabine was dissolved in sterile saline to achieve a concentration of 5 mg/ml. The
116 solution was freshly prepared immediately prior to use. For intraperitoneal (IP) injection, mice
117 received Tiagabine at a dosage of 10 mg/kg body weight. Control animals were administered an
118 equivalent volume of sterile saline.

119 **Surgery and electrode implantation**

120 Mice were administered analgesic (buprenorphine, 0.5 mg/kg, subcutaneous) 30 min before
121 surgery, and anesthesia was maintained with isoflurane (1–2% in O_2). After scalp removal, a small
122 craniotomy (~2.6 mm lateral to midline, posterior to occipital suture) was made in the right
123 hemisphere for hippocampal electrode implantation. A bipolar hippocampal electrode (two twisted
124 50 μm Teflon-coated stainless-steel wires; A-M Systems) was slowly inserted through the
125 craniotomy at a 57° angle relative to vertical, guided by continuous visual and auditory signal
126 quality monitoring. Once optimal placement was confirmed, the electrode was secured using
127 Krazy Glue and dental cement. Additionally, an EMG electrode was implanted into neck muscles.

128 A custom head plate was fixed to the skull for head restraint, and the skull surface was sealed with
129 Metabond (Parkell, Inc.) and a glass coverslip to create a cranial window for cortical imaging.
130 Animals recovered for two weeks before recordings commenced.

131 **iGABASnFR2 imaging under anesthesia**

132 Seven days post-surgery, the animals were anesthetized with isoflurane (2.5% for induction,
133 followed by 1% for maintenance). The depth of anesthesia was confirmed by assessing reflexes.
134 Once adequately anesthetized, each mouse was positioned in a head-stage, and the head was
135 securely head-fixed. A homoeothermic blanket was utilized to maintain their body temperature,
136 and isoflurane was administered via a nosepiece. The isoflurane concentration was adjusted to 1%
137 to initiate the imaging procedure. Images were acquired using a microscope consisting of a front-
138 to-front pair of video lenses with a field of view measuring 8.6 × 8.6 mm. The camera's focal plane
139 was positioned 0.5–1 mm (about 0.04) below the cortical surface. A 12-bit charge-coupled device
140 (CCD) camera (1M60 Pantera Dalsa, Waterloo, ON) and an EPIX E8 frame grabber with XCAP
141 3.8 imaging software (EPIX, Inc., Buffalo Grove, IL) were employed to capture the images at a
142 frame rate of 80 Hz. These imaging parameters have been utilized in prior investigations, such as
143 voltage-sensitive dye imaging (Mohajerani et al.,2013), anesthesia-induced GCaMP3 imaging to
144 observe spontaneous activity in the mouse cortex (Vanni et al.,2014), and awake GCaMP6 imaging
145 in the mouse cortex utilizing a chronic window (Silasi et al.,2016). The thoroughness of our data
146 collection methodology ensures the reliability of our results. Sequential illumination of the cortex
147 occurred with meticulously controlled alternating blue and green LEDs (Xiao et al.,2021)
148 (Thorlabs). Blue light (473 nm) with a bandpass filter (467 to 499 nm) was applied to excite
149 iGABASnFR2 indicators, while green light (530 nm) with a bandpass filter (527⁄42 nm) was used
150 to observe changes in cerebral blood volume in alternating images. The activation of blue and
151 green LEDs was synchronized and sequentially activated at the start of each frame's exposure
152 period through transistor-transistor logic. This ensured that each frame exclusively collected
153 fluorescence or reflectance signals at a rate of 40 Hz each. Additionally, images of reflectance,
154 crucial for blood artifact corrections, were evaluated within the current pipeline. Anesthetized
155 iGABASnFR2 imaging of spontaneous activity was conducted without sensory stimulation for 15-
156 minute sessions.

157 **Sensory stimulation**

158 We captured the iGABASnFR2 signal in reaction to varied peripheral simulations while utilizing
159 urethane anesthesia, following the methodology outlined in previous studies. Sensory stimuli were
160 employed to map the functional areas of the hind-limb somatosensory, forelimb somatosensory,
161 auditory, visual, and barrel cortices (Mohajerani et al.,2013; Navvab et al.,2021). Sensory stimuli
162 were applied to map cortical regions corresponding to forelimb, hindlimb, whisker, visual, and
163 auditory modalities. For forelimb and hindlimb stimulation, a piezoelectric bending actuator
164 delivered a single 300-ms tap via a square pulse directly to the skin of one forelimb or hindlimb.
165 Whisker stimulation targeted the C2 whisker, which was attached to a piezoelectric actuator
166 (Q220-A4-203YB, Piezo Systems, Inc., Woburn, MA) and stimulated by a single 300-ms square
167 pulse. This resulted in whisker movement of up to 90 µm in an anterior-to-posterior direction,
168 corresponding to approximately a 2.6° deflection angle. Visual stimuli consisted of a single 20-ms
169 pulse of light (435 nm LED) presented at a consistent distance and height relative to the right eye.
170 For each sensory modality, 40 stimulus presentations were delivered with a 10-second
171 interstimulus interval to calculate average cortical responses.

172 **Habituation**

173 After the 14-day recovery period from surgery, mice gradually habituated to head restraint in the
174 recording environment. Initially, each mouse was placed individually on the recording platform
175 along with Cheerios cereal, allowing them to explore freely and become comfortable. Mice were
176 progressively acclimated to eating the cereal while head-fixed, beginning with 5-minute sessions
177 and increasing by 5 minutes each day until reaching 60 minutes.

178 **iGABASnFR2 imaging during wakefulness**

179 Following habituation, wakefulness recordings began. Each animal underwent recording sessions
180 every three days, completing three to four sessions per mouse. Recordings were consistently
181 performed at the same time of day to reduce variability and stress. Between sessions, mice were

returned to their home cages for rest and recovery before the next recording. After finishing all wakefulness sessions, mice proceeded to the sleep recording phase.

iGABASnFR2 imaging during sleep

To optimize conditions for natural sleep under head restraint, mice were transferred from their colony housing to a separate room at noon the day before recording. Sleep was then restricted for approximately six hours by gentle stimulation (using a cotton-tip stick) whenever signs of drowsiness were observed, occasionally combined with gentle handling in the final hours. Following sleep restriction, animals were placed overnight in larger cages enriched with objects (e.g., running wheel, Cheerios, and water container) to encourage exploration and natural sleep afterward. The next day, at approximately 9:00 AM, mice were transferred to the recording platform, and sleep recordings commenced. Afterward, mice returned to their home cages in the colony room to recover freely for at least three days before any subsequent recordings.

preprocessing

Wide-field imaging data collected using the iGABASnFR2 sensor underwent preprocessing to prepare for further analysis. Imaging was conducted using alternating blue (470 nm) and green (530 nm) illumination at a sampling rate of 80 Hz, with raw data stored as .tif files. Image stacks were first de-interleaved to isolate fluorescence (green channel) and reflectance (blue channel) signals. The correct channel order was identified by comparing the first frame of each stack to reference images from green and blue channels using pixel-wise correlation. Fractional fluorescence changes ($\Delta F/F$) were computed for each pixel using a 2-second pre-stimulus period as baseline fluorescence (F_0). Specifically, $\Delta F/F$ was calculated by subtracting the baseline fluorescence from the instantaneous fluorescence and dividing by the baseline, ensuring consistency across trials. A pixel-wise regression approach was applied to remove hemodynamic artifacts, subtracting a scaled reflectance signal from the fluorescence signal, thus yielding a corrected $\Delta F/F$ signal largely free from blood flow noise. This corrected signal was subsequently bandpass filtered (31–74 Hz) using a second-order Butterworth filter, effectively eliminating low-frequency drift and high-frequency artifacts. Trial-averaged $\Delta F/F$ responses were then generated

for sensory-evoked analysis. All preprocessed data (corrected ΔF/F, fluorescence, and reflectance signals) were saved as ". float32" files.

ROI-based fluorescence analysis

Following preprocessing, fluorescence data from specific regions of interest (ROIs)—defined as 3×3-pixel areas centered around anatomical coordinates corresponding to stimulation sites—were extracted and reshaped into 2D matrices for streamlined analysis. Baseline correction was conducted by subtracting the mean fluorescence calculated from a 1-second pre-stimulus period from the post-stimulus fluorescence signals. The signals underwent additional filtering to remove slow drifts (high-pass, above 0.1 Hz) and high-frequency noise (low-pass, below 5 Hz). From the filtered signals, several key parameters were derived, including peak amplitude (maximum $\Delta F/F_0$ within a 1-second post-stimulus interval), time-to-peak, and decay time (duration for the fluorescence to fall to 50% of peak amplitude). Additional metrics calculated per trial included signal-to-noise ratio (SNR) and rise time (10–90% of peak amplitude). For visualization, the corrected $\Delta F/F_0$ signals were plotted with indicators marking peak and decay times, facilitating clear interpretation of response dynamics. Mean responses across trials were computed separately for each sensory modality, with variability assessed by plotting the standard error of the mean (SEM) as shaded regions surrounding the mean trace. Data windows were constrained to periods from 400 ms pre-stimulus to 1 second post-stimulus, enabling detailed characterization of the GABAergic response. Finally, contralateral and ipsilateral cortical responses were averaged and directly compared to reveal hemispheric dynamics in GABAergic activity.

Seed-pixel correlation analysis

Seed pixel correlation analysis was performed to evaluate functional connectivity based on spontaneous neural activity from sleep and anesthetized mice. preprocessed data were spatially registered to the Allen Brain Atlas, enabling anatomical alignment and inter-subject comparisons. Regions of interest (ROIs)—specifically the barrel cortex (BC), visual cortex (VC), hindlimb (HL), and forelimb (FL)—were defined using anatomical coordinates derived from the atlas. Within each ROI, seed pixels were selected to serve as reference points for correlation-based connectivity analysis.

Motion detection and exclusion

Motion artifacts were identified and excluded from analyses using electromyography (EMG) signals recorded simultaneously with imaging data. EMG recordings were smoothed using a median filter and squared to enhance the detection of muscle activity periods. An activity threshold was established at the 85th percentile of the processed EMG signal to identify movement onset and offset events. These EMG-detected motion periods were temporally aligned with imaging frames via synchronized camera clock signals. Frames coinciding with detected movements were subsequently removed from analysis, ensuring the seed pixel correlation analysis reflected only stationary periods free of motion-related artifacts.

Correlation coefficient analysis

Following the exclusion of motion-affected frames, a finite impulse response (FIR) bandpass filter with cutoff frequencies of 0.1-5 Hz was applied to the fluorescence signals to remove low-frequency drifts and high-frequency noise. The filtering step was essential to ensure the functional connectivity analysis focused on the relevant frequency bands for spontaneous neural activity. Time series were extracted from the seed pixels within each ROI, and Pearson correlation coefficients were calculated between the seed pixel time series from different regions. The analysis mainly focused on interhemispheric correlations between homologous regions in the left and right hemispheres, indicative of functional connectivity between corresponding areas across both sides of the brain.

Sleep scoring

Sleep stages were classified into wakefulness, NREM sleep, and REM sleep based on a combination of behavioral observations and physiological signals, including EMG activity and hippocampal theta-to-delta power ratios. Wakefulness was characterized by high EMG activity and visual confirmation of movement. NREM sleep was identified by low EMG activity and a low theta-to-delta ratio, indicating reduced cortical arousal. In head-restrained experiments, an additional criterion for NREM sleep classification was the absence of facial movement,

263 particularly around the chin, for a duration of at least 50 seconds. REM sleep, marked by muscular
264 atonia, was detected through minimal EMG activity and a high theta-to-delta ratio, consistent with
265 its distinct physiological signature. For head-fixed experiments, pupil size was also monitored as
266 an auxiliary measure to validate sleep stage classifications, as pupil constriction correlates with
267 sleep states (Yüzgeç et al., 2018). This multi-modal approach ensured accurate classification of
268 vigilance states in both freely moving and head-restrained animals.

269 **Statistical analysis**

270 All data processing and analyses were performed using custom scripts written in MATLAB
271 R2024a. Signal processing functions such as filtering and correlation computations utilized
272 MATLAB's built-in functions and Signal Processing Toolbox. The FIR bandpass filter was
273 designed using the design file function with specified parameters to achieve the desired frequency
274 characteristics. Statistical analyses involved calculating Pearson correlation coefficients and
275 generating correlation matrices. The results were visualized using MATLAB's plotting functions,
276 with custom formatting to enhance readability. The correlation matrix heatmap included numerical
277 annotations of the correlation values and graphical elements to delineate different regions.

278 **Results**

279 **Experimental workflow, imaging setup, and cortical expression of iGABASnFR2**

280

281 To characterize extracellular GABA dynamics using iGABASnFR2, we employed a wide-field
282 imaging approach in head-fixed mice, systemically expressing the sensor via retro-orbital
283 AAV2/PHP.N injection. As illustrated in (**Figure 1A**), the experimental timeline included viral
284 delivery at 6 weeks of age, followed by a four-week expression period, chronic cranial window
285 implantation, and two weeks of habituation before imaging. We recorded iGABASnFR2
286 fluorescence under isoflurane anesthesia, during quiet wakefulness, and throughout natural sleep
287 over several weeks, followed by histological analysis. The imaging setup (**Figure 1B**) featured a
288 bilateral cranial window preparation and a CCD-based wide-field microscope that captured
289 fluorescence across an 8.6 × 8.6 mm field of view. Sequential blue (470 nm) and green (530 nm)
290 LED illumination enabled alternating frames for GABA signal acquisition and hemodynamic
291 correction. To confirm sensor expression, we performed histological analysis (**Figure 1C**), which

revealed strong iGABASnFR2 fluorescence in cortical and hippocampal regions. Coronal sections (**Figure 1Cii**) demonstrated widespread and consistent expression across animals. To assess inter-animal variability and regional expression strength, fluorescence intensity profiles were extracted using ImageJ across defined cortical areas (**Figure 1Ciii**), confirming uniform sensor expression suitable for quantitative cortical imaging.

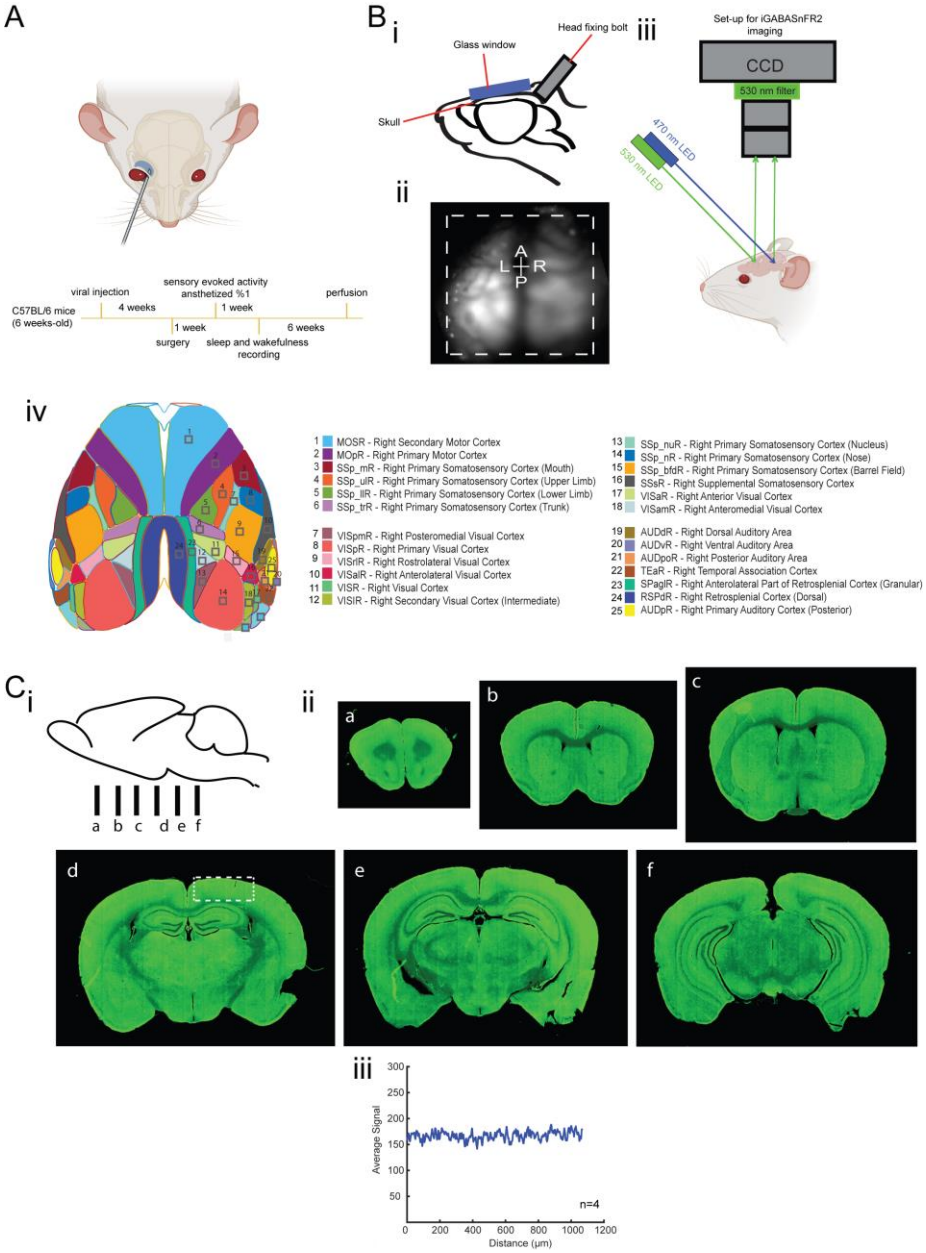

Figure 1. Schematic of experimental workflow, imaging setup, and an expression of iGABASnFR2. A. Experimental timeline. AAV2/PHP.N-CAG-iGABASnFR2 or the control virus AAV2/PHP.N-CAG-csGFP was systemically administered via retro-orbital injection into 6-week-old C57BL/6 mice. Four weeks post-injection, mice underwent chronic cranial window implantation. After a two-week recovery and habituation period, sensory-evoked activity was

recorded under 1% isoflurane anesthesia. One week later, longitudinal recordings during wakefulness and natural sleep were performed for up to six weeks. Mice were subsequently euthanized, and brains were perfused for histological analysis. Imaging setup. (i). Illustration of the cranial window implantation over the skull following scalp removal. (ii). A representative image showing the cortical imaging area, indicated by the dashed white line. (iii). Schematic of the wide-field imaging setup: a blue LED (470 nm) was used for excitation, and signals were captured using a CCD camera at 530 nm emission. (iv). Map of the bilateral craniotomy showing targeted cortical regions based on Allen Mouse Brain Atlas reference. C. expression of iGABASnFR2. (i). Schematic of coronal sectioning locations (a–f) along the anterior-posterior axis. (ii). Coronal sections (a–f) show strong iGABASnFR2 expression in the cortex and hippocampus. (iii). The region marked by a white dashed rectangle in panel C(iid) was used to extract fluorescence profiles across animals (n=4), highlighting unique expression and inter-animal expression consistency.

iGABASnFR2 reveals modality- and hemisphere-specific cortical inhibition under anesthesia

Previous studies on sensory processing have primarily focused on excitatory neuronal responses, often using calcium or glutamate indicators to map stimulus-evoked activity across the cortex (Chen et al., 2013; Xie et al., 2016; Mohajerani et al.,2013). However, much less is known about how sensory stimuli engage inhibitory networks, particularly at the mesoscale. Inhibitory interneurons play a crucial role in shaping sensory responses, modulating cortical excitability, and controlling the timing and precision of neural coding (Atallah et al., 2012; Wilson et al., 2012). To examine the spatiotemporal dynamics of GABA activity across the cortex, we delivered contralateral whisker, hindlimb, forelimb, and visual stimulation under 1% isoflurane anesthesia and recorded GABA activity using the iGABASnFR2 sensor. Imaging was performed at 80 Hz using a dual-wavelength strobing protocol, where blue and green excitation LEDs alternated between consecutive frames to avoid spectral contamination. The timing of the LED alternation and stimulus delivery is illustrated in **Supplementary Figure 1.** As shown in (**Figure 2A**), each sensory modality evoked a localized increase in GABAergic fluorescence in the corresponding primary sensory cortex, with responses initiating around 75–150 ms post-stimulus. All sensory modalities elicited more robust and spatially localized GABAergic activity. Temporal response profiles (**Figure 2B**) demonstrated stronger GABAergic activation in the contralateral hemisphere relative to the ipsilateral side across all sensory modalities. Specifically, the contralateral visual cortex exhibited the highest peak amplitude (~0.34 ΔF/F), followed by hindlimb (~0.26), whisker (~0.2), and forelimb (~0.16) cortices. Ipsilateral responses were generally weaker and slower, with the visual cortex being an exception—showing a relatively strong response (~0.3 ΔF/F) but with

339 an extended decay phase, suggesting prolonged inhibition. To quantify these differences, we
340 extracted response features including decay time, time to peak, and peak amplitude across all
341 sensory regions and hemispheres (**Figure 2C**). A two-way ANOVA revealed significant main
342 effects of sensory region on decay time ($p = 0.0479$), peak amplitude ($p = 0.0048$), and time to
343 peak ($p < 0.0001$), confirming region-specific variation in inhibitory response dynamics. Laterality
344 significantly affected peak amplitude ($p = 0.0076$), while a significant Region × Laterality
345 interaction was found for time to peak ($p = 0.0055$), indicating that hemispheric differences in
346 GABAergic responses were modality dependent. To confirm that these delayed signals were
347 specific to GABAergic dynamics and not artifacts of hemodynamics or sensor excitation, we used
348 csGFP-expressing mice under identical imaging conditions as a negative control. As shown in
349 **Supplementary Figure 2**, csGFP mice exhibited no significant sensory-evoked or spontaneous
350 fluorescence changes in response to the same stimuli or during baseline, confirming that the
351 iGABASnFR2 signals reflect genuine GABAergic activity. Additionally, GABAergic responses
352 to auditory stimulation were consistent with other sensory modalities, showing a delayed
353 fluorescence increase in the contralateral auditory cortex under anesthesia **Supplementary Figure**
354 **3**, supporting the generality of late GABAergic feedback across sensory systems. We calculated
355 intrahemispheric functional connectivity by performing seed-pixel correlation analysis across 10
356 defined cortical regions to further examine cortical coordination during sensory processing. This
357 analysis revealed highly structured and modality-specific inhibitory networks, with the strongest
358 connectivity typically observed in the hemisphere contralateral to the stimulated side
359 **Supplementary Figure 4**. Across sensory modalities—including whisker **(Video 1)**, hindlimb
360 **(Video 2)**, forelimb **(Video 3)**, and visual **(Video 4)** stimulation—sensory input activates
361 thalamocortical projections targeting layer 4 of the primary sensory cortices, leading to early
362 excitatory responses (Petersen, 2007; Ridder & Nusinowitz, 2006). These are primarily mediated
363 by excitatory neurons and refined by fast feedforward inhibition from parvalbumin (PV)-
364 expressing interneurons (Gabernet et al., 2005; Isaacson & Scanziani, 2011). Subsequently, a
365 delayed GABAergic response emerges, largely driven by somatostatin (SST)-expressing
366 interneurons providing feedback inhibition to modulate dendritic activity and maintain cortical
367 stability (Muñoz et al., 2017; Gentet et al., 2012; Urban-Ciecko & Barth, 2016). This response is
368 consistently stronger and earlier in the contralateral hemisphere, which receives direct thalamic
369 input, whereas the ipsilateral hemisphere exhibits a weaker and more delayed GABAergic
370 response, likely due to slower callosal transmission and reduced excitatory drive (Ferezou et al.,

2007; Minamisawa et al., 2018). Despite regional differences, this temporal pattern—early excitation followed by delayed inhibition—is a conserved cortical mechanism ensuring precise and balanced sensory processing. Together, these findings demonstrate that sensory-evoked GABA dynamics follow a consistent temporal structure across modalities and hemispheres, characterized by rapid excitation followed by spatially and temporally regulated inhibition. These findings also demonstrate that iGABASnFR2 can reliably detect stimulus-evoked extracellular GABA responses with spatiotemporal precision across multiple cortical regions, confirming its utility for mapping inhibitory dynamics at the mesoscale.

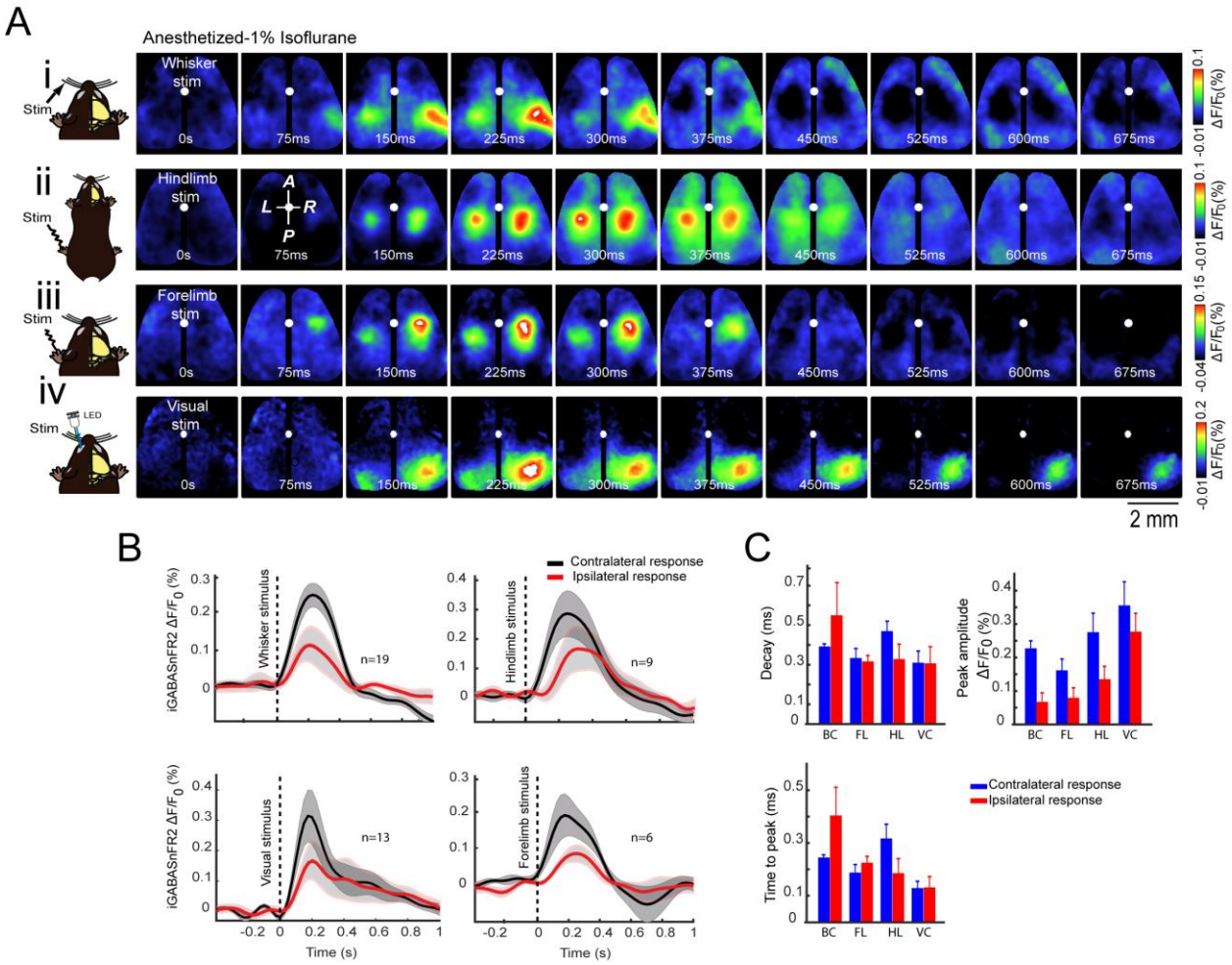

Figure 2. Sensory-evoked GABAergic responses in the neocortex measured by iGABASnFR2 imaging. A. Montages of the wide bilateral craniotomy, with bregma marked by a white circle. Cortical GABAergic activation patterns are shown in a mouse anesthetized with isoflurane (1%) following: (i) whisker stimulation (300 ms), (ii) hindlimb stimulation (300 ms), (iii) forelimb stimulation (300 ms), and (iv) visual stimulation (20 ms) of the eye using an LED. Sensory-evoked extracellular GABA signals were detected using the iGABASnFR2 sensor. Activation is observed within 50–375 ms post-primary sensory cortex activation. Responses represent an average of 40 trials. The second image in the second row indicates anterior (A), posterior (P), medial (M), and

lateral (L) directions. B. Time series of sensory-evoked GABA responses. The time series of GABA responses for each sensory stimulation was measured from the respective primary sensory regions. Contralateral responses are shown in black, and ipsilateral responses are shown in red. Data are presented as mean ± SEM, with responses extracted from 3 × 3-pixel regions of interest (ROI) (~0.04 mm^2), n = number of animals. C. Summary of sensory-evoked GABA response features. Decay time (ms), Peak amplitude (ΔF/F) and Time to peak (ms) for contralateral and ipsilateral responses. Data are shown as mean ± SEM, with contralateral responses in blue and ipsilateral responses in red. Statistical Analysis (Two-Way ANOVA): A two-way ANOVA revealed a significant effect of Region on decay time ($p = 0.0479$), peak amplitude ($p = 0.0048$), and time to peak ($p < 0.0001$), indicating sensory-region-dependent differences in GABA responses. Laterality (contralateral vs. ipsilateral) significantly affected peak amplitude ($p = 0.0076$) but not decay time ($p = 0.9874$) or time to peak ($p = 0.5535$). A significant Region × Laterality interaction was found for time to peak ($p = 0.0055$), indicating lateralization effects vary across sensory regions.

Sensory-evoked and spontaneous GABA activity in quiet wakefulness resembles anesthesia-induced patterns

Cortical brain states vary across behavioral conditions, shaping spontaneous activity and sensory processing. During active behavior, such as locomotion or whisking, cortical activity becomes desynchronized, and inhibition is modulated to refine sensory gain (Pakan et al., 2016 & 2018; Gentet et al., 2010; Keller et al., 2018). In contrast, during quiet wakefulness and under light anesthesia, neuronal activity is dominated by slow, synchronized fluctuations that reflect reduced arousal and a shift toward global inhibitory tone (McGinley et al., 2015; Muñoz et al., 2017). While previous studies have shown that GABAergic interneurons contribute significantly to these state-dependent dynamics (Chen et al., 2012; Pfeffer et al., 2013), it remains unclear whether the spatiotemporal profile of extracellular GABA during quiet wakefulness resembles that observed under anesthesia. To examine whether GABAergic responses to sensory stimulation and spontaneous activity in quiet awake mice exhibit spatiotemporal dynamics similar to those observed under anesthesia, we performed wide-field imaging of the cortex using the iGABASnFR2 sensor. Head-fixed mice were imaged in both quite awake and anesthetized states, the latter induced by 1% isoflurane. EMG recordings from a neck muscle electrode, along with video monitoring of body and whisker movement, were used to classify behavioral state (**Figure 3A**). Power spectral analysis of EMG signals confirmed a reduction in muscle tone under anesthesia compared to the quiet awake state. We recorded cortical GABA signals evoked by contralateral visual or whisker stimulation, averaging responses across 40 trials for each condition (**Figure 3B**). Both anesthetized and quiet awake states showed robust stimulus-evoked increases in extracellular GABA in primary sensory areas, including the primary visual cortex (VISp),

anterior visual area (VISa), barrel cortex (BC), and primary motor cortex (M1). The spatial spread and time series of GABA signals were largely conserved across states. Quantitative analysis of GABA responses from defined 3×3-pixel ROIs (~0.04 mm^2) revealed no major differences in response dynamics across states (**Figure 3C**). Peak amplitude, time to peak, and decay time of sensory-evoked GABA transients in VISp and VISa (visual stimulation) and BC and M1 (whisker stimulation) were statistically comparable between anesthetized and quiet awake mice (**Figure 3D**). These findings suggest that, similar to previously reported glutamatergic dynamics, GABAergic activity patterns in response to sensory input are preserved across brain states, indicating stereotypical and robust cortical inhibitory responses regardless of anesthesia (Xie et al., 2016).This state-invariant pattern further supports the reliability of iGABASnFR2 in capturing stable and reproducible extracellular GABA signals under varying levels of arousal, validating its utility for longitudinal studies of cortical inhibition.

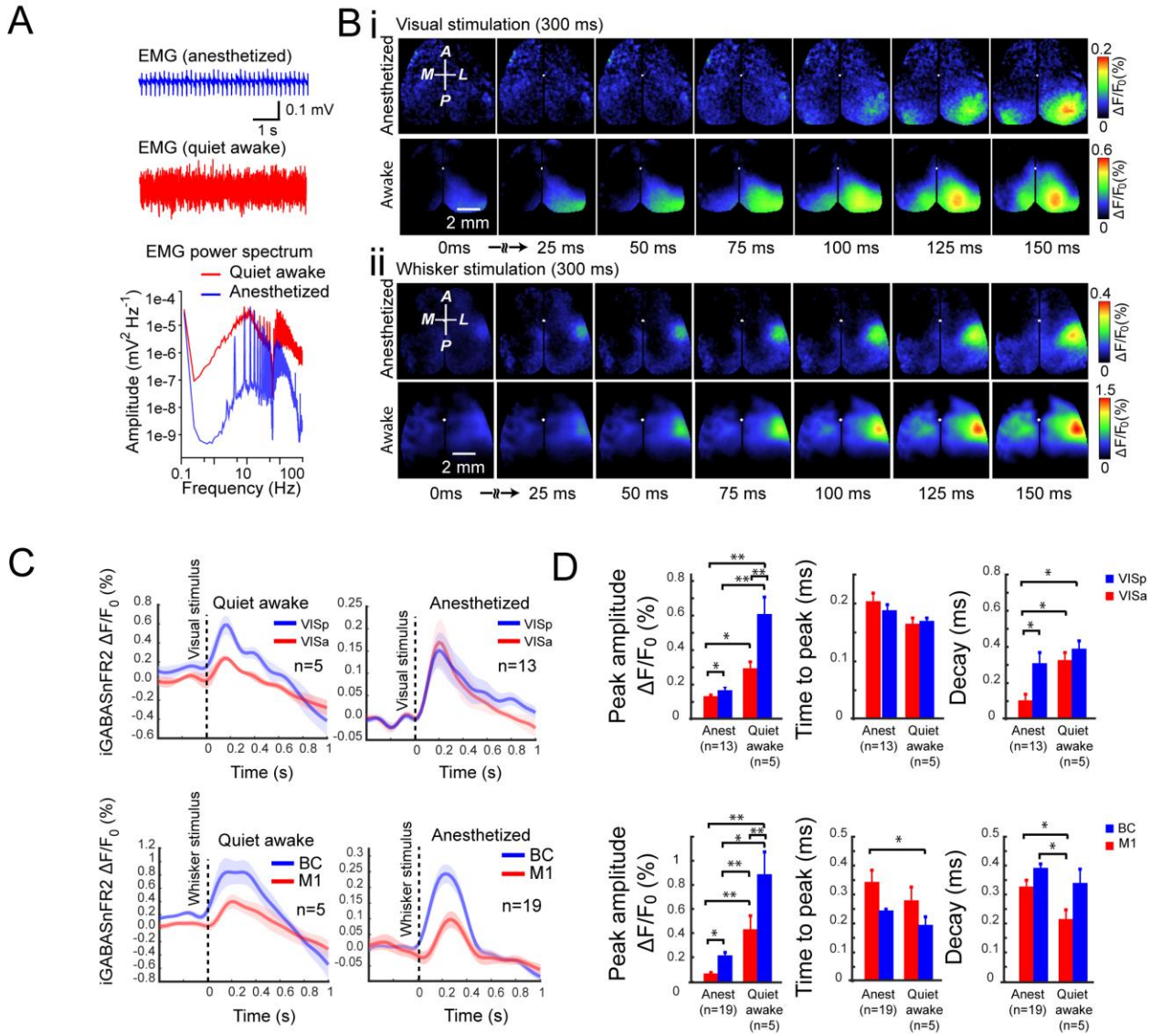

Figure 3. Sensory-evoked and spontaneous GABA activity in quiet wakefulness resembles patterns observed under anesthesia. (A) Individual example of neck muscle EMG (>1 Hz) from a head-restrained mouse under isoflurane (1%) anesthesia (top trace) and quite awake (bottom trace). The power spectra of the EMG signals differ between states of anesthesia (blue) and wakefulness (red). (B) Representative cortical GABA signals are taken from the iGABASnFR2 sensor in response to contralateral visual or whisker stimulation during anesthesia or in quiet awake states. The images represent an average of 40 trials of stimulation (C) Quantification of GABA signals in response to sensory stimulation under anesthesia and quiet wakefulness. Plots show averaged responses from 3 × 3-pixel ROIs (~0.04 mm²) within VISp (blue) and VISa (red) for visual stimulation and BC (blue) and M1 (red) for whisker stimulation (Ciii, Civ). Shaded areas represent SEM. (D) Statistical comparison of peak amplitude, time to peak, and decay time of GABA responses across states. *P < 0.05, **P < 0.01, one-way ANOVA. Error bars indicate SEM.

Mesoscale imaging of cortical GABA dynamics during natural sleep and wakefulness

While many studies have explored cortical dynamics across sleep and wake states using electrophysiological methods and excitatory activity sensors (Dash et al., 2009; Karimi Abadchi et al., 2020; Nazari et al.,2023; Karimi Abadchi et al.,2023), the ability to track inhibitory signaling at mesoscale resolution across natural brain states remains limited. To address this gap and to further validate the performance of the iGABASnFR2 sensor under diverse physiological conditions, we investigated cortical GABA dynamics during quiet wakefulness, non-rapid eye movement (NREM) sleep, and rapid eye movement (REM) sleep. This analysis allowed us to assess whether iGABASnFR2 could reliably capture spontaneous fluctuations in extracellular GABA levels across distinct behavioral states. We combined mesoscale iGABASnFR2 imaging with simultaneous hippocampal LFP and EMG recordings in head-fixed mice. Mice were allowed to naturally transition between quiet wakefulness, NREM, and REM sleep while we monitored changes in cortical GABA levels and brain state (**Figure 4A–C**). EMG power and hippocampal LFP confirmed behavioral state classification, with NREM sleep characterized by high-amplitude slow oscillations (0.1–5 Hz) and REM sleep by prominent theta band activity (7–9 Hz). Across the dorsal cortex, we observed distinct spatiotemporal patterns of GABA activity during each brain state (**Figure. 4A**). Notably, GABA signals were higher during wakefulness and NREM sleep but significantly reduced during REM sleep (**Figure 4D**). Spectral analysis of GABA signals revealed reduced low-frequency fluctuations in REM compared to wakefulness and NREM (**Figure 4E**), indicating decreased slow cortical GABA oscillations during REM sleep. To further assess spatial coordination of cortical GABA activity, we computed pairwise correlation maps across the cortex during each brain state over multiple days. As shown in (**Figure 4F**), cortical GABA signals during quiet wakefulness and NREM exhibited strong bilateral synchrony, which was significantly diminished in REM sleep (**Figure 4G**). These results are consistent with previous findings of reduced functional connectivity during REM sleep (Rynes et al., 2021). Finally, we examined the transition from REM sleep to wakefulness and observed a striking increase in cortical GABA levels (**Figure 4H**), coinciding with hippocampal theta-to-desynchronized LFP shift and EMG activation. This transition was accompanied by a broad re-engagement of cortical GABAergic activity across multiple regions (**Figure 4I**), suggesting rapid reinstatement of GABA response upon arousal from REM sleep. A detailed overview of the motion-based and electrophysiological features used for behavioral state classification is provided in **Supplementary Figure 5**, which illustrates the temporal alignment of whisker pad and nose motion, EMG power, body motion, theta-to-delta ratio, and hippocampal LFP signals across NREM and REM sleep

transitions.Together, these findings demonstrate that iGABASnFR2 reliably captures spontaneous, brain state-dependent fluctuations in extracellular GABA with high temporal and spatial resolution. It supports its utility for long-term mesoscale imaging of cortical inhibition under natural physiological conditions.

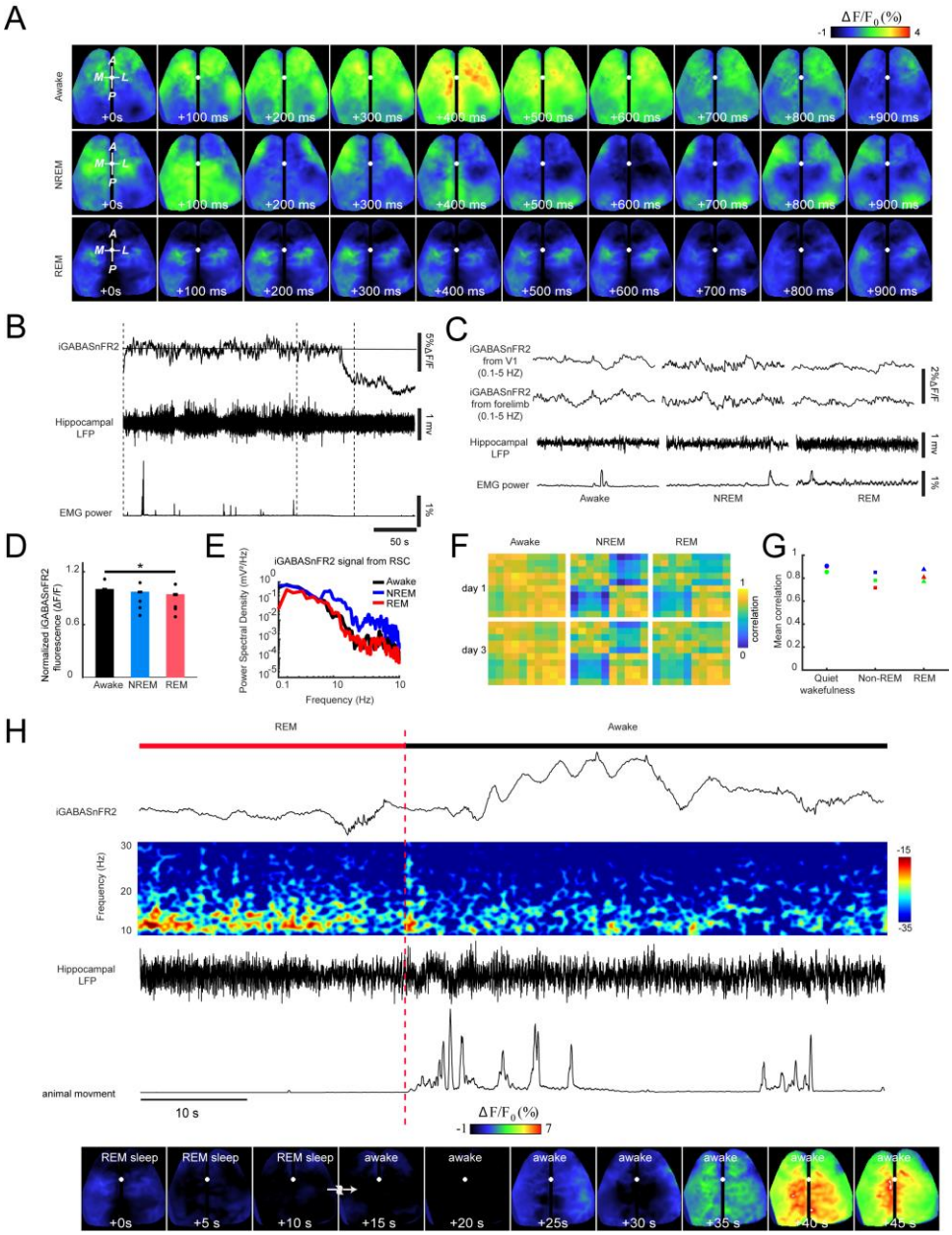

Figure 4. Combined electrophysiological recording and mesoscale iGABASnFR2 imaging of GABA activity during wakefulness and sleep. (A) Spatiotemporal dynamics of GABA activity over a 1-s period during wakefulness, NREM, and REM sleep. Scale bar, 2 mm. (B) Representative traces of GABA activity (RSC), hippocampal LFP, and EMG power during wakefulness, NREM, and REM sleep in a head-fixed mouse. Baseline fluorescence (F_0) was calculated as the mean

signal over the recording session. (C) Expanded view of GABA activity, LFP, and EMG power corresponding to the time windows in (B). (D) Group mean normalized GABA signal across wakefulness, NREM, and REM sleep (n = 5 mice, Friedman test with Dunn's post hoc correction; $P < 0.05$ for wakefulness vs. REM, $P = 0.04$). (E) Spectral power of GABA signal in retrosplenial cortex (RSC) across wakefulness, NREM, and REM sleep. (F) Cortical GABA activity correlation maps across quiet wakefulness, NREM, and REM sleep over two recording days. (G) Mean correlation of cortical activity during wakefulness, NREM, and REM sleep (n = 5 mice). (H) GABA activity, hippocampal LFP spectrogram, and EMG power during REM-to-wakefulness transition. (I) Montage of cortical GABA changes during REM-to-wake transition shown in (H). Scale bar, 2 mm.

Intracortical long-range GABAergic correlations revealed by seed-pixel analysis across brain states

To assess the organization of spontaneous extracellular GABA dynamics in the cortex, we used seed-pixel correlation mapping of iGABASnFR2 fluorescence to investigate intracortical long-range connectivity across different brain states. By placing seed pixels in primary sensory regions—barrel cortex (BC), forelimb (FL), hindlimb (HL), and visual cortex (VC)—we generated correlation maps of spontaneous GABA dynamics in awake, NREM, and REM sleep conditions (**Figure 5A**). In the awake state, seed-pixel correlation maps revealed robust bilateral synchrony and widespread long-range connectivity between distant cortical regions. This was especially evident in primary sensory cortices, where interhemispheric homologs and surrounding association areas exhibited high correlation values. These spatial patterns of functional connectivity closely resemble those previously observed with excitatory signals using iGluSnFR and Ca^{2+} imaging, suggesting that spontaneous GABA activity also reflects underlying anatomical connectivity and shared network drive (Silasi et al., 2014; Vanni & Murphy, 2014; Navvab et al.2021). During NREM sleep, seed-pixel correlations were notably reduced, particularly in long-range and interhemispheric connections, indicating a decoupling of large-scale inhibitory networks during cortical slow-wave activity. In contrast, REM sleep preserved many of the bilateral and local connections seen in wakefulness, although with moderate reductions in correlation strength. We further quantified interhemispheric connectivity using pairwise correlation matrices of bilateral cortical regions (**Figure 5B**). During quiet wakefulness and REM sleep, strong correlations were observed between corresponding motor, somatosensory, and visual regions. However, during NREM sleep, functional connectivity was significantly diminished across nearly all regions, especially in lateral sensory areas such as SSp_ul, VISp, and VISpm. Together, these results demonstrate that spontaneous extracellular GABA activity, like glutamatergic activity

(Rynes et al., 2021), reveals a dynamic and brain-state-dependent pattern of intracortical long-range connectivity. The high degree of bilateral synchronization during wakefulness and REM sleep, contrasted with reduced connectivity in NREM, underscores the role of GABA dynamics in shaping the functional architecture of the cortex during sleep-wake transitions. These patterns, reliably detected using iGABASnFR2, highlight the sensor's sensitivity to spontaneous, state-dependent fluctuations in extracellular GABA and its capacity to reveal mesoscale functional inhibitory architecture in vivo.

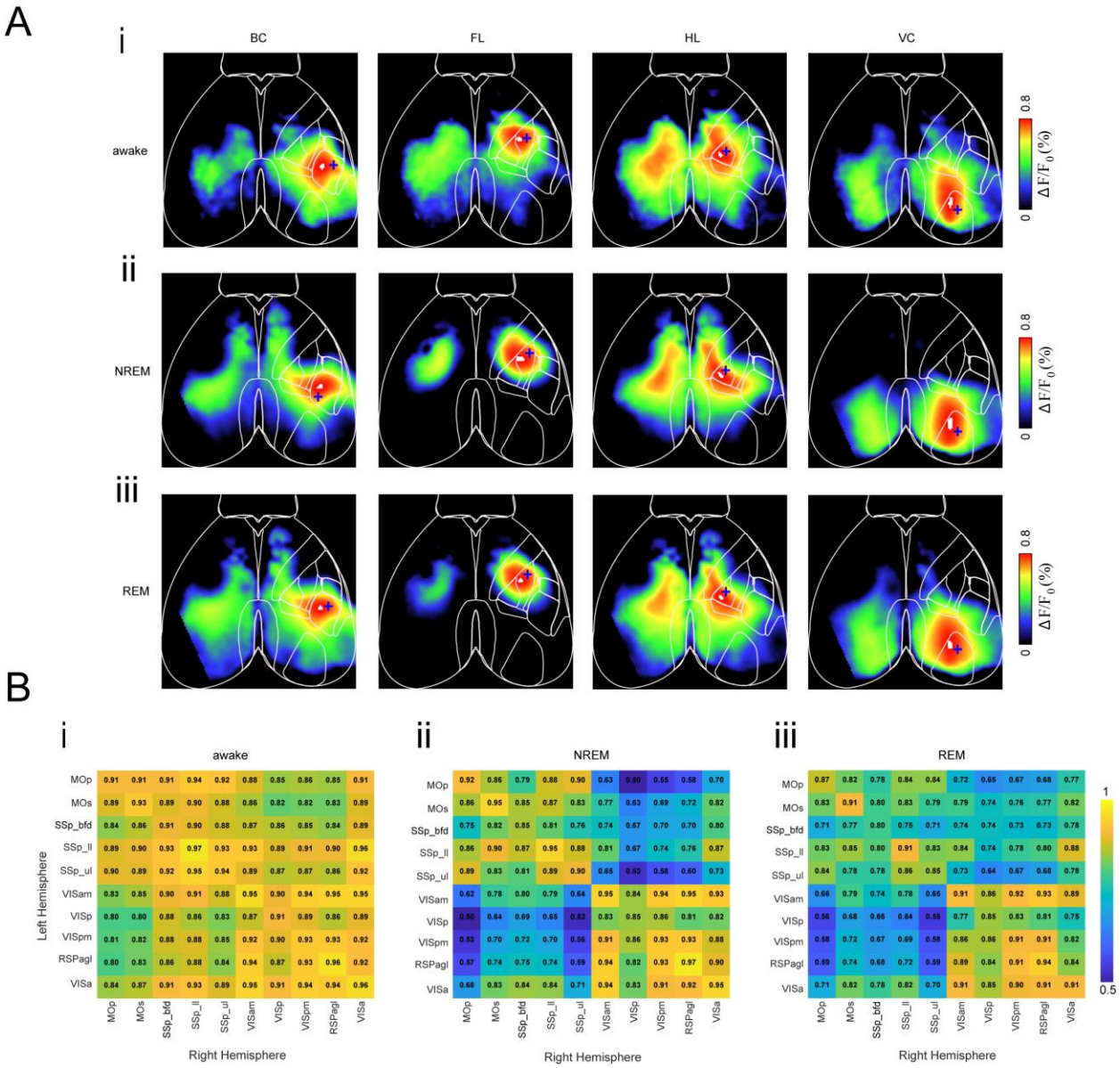

Figure 5. Brain state–dependent patterns of extracellular GABA dynamics measured by iGABASnFR2. (A) Seed-pixel correlation maps (0.1–5Hz) of spontaneous iGABASnFR2 fluorescence across brain states. (i) Awake, (ii) NREM sleep, and (iii) REM sleep. Correlation

maps are shown for seed regions in the barrel cortex (BC), forelimb cortex (FL), hindlimb cortex (HL), and visual cortex (VC). (B) Interhemispheric correlation matrices of spontaneous extracellular GABA signals across brain states. (i) Awake, (ii) NREM sleep, and (iii) REM sleep. Matrices display Pearson correlation coefficients between bilateral cortical regions based on iGABASnFR2 fluorescence. Regions include: MOp – Primary motor area, MOs – Secondary motor area, SSp_bfd – Primary somatosensory area (barrel field), SSp_ll – Lower limb, SSp_ul – Upper limb, VISam – Anteromedial visual area, VISp – Primary visual area, VISpm – Posteromedial visual area, RSPagl – Agranular retrosplenial area, VISa – Anterior visual area. Widespread interhemispheric connectivity is observed during wakefulness and REM sleep, with reduced correlation during NREM sleep. Blue crosses indicate the location of the seed pixel used for correlation mapping. number of animals=5.

Tiagabine elevates baseline GABA levels but dampens sensory-evoked responses and reorganizes cortical inhibitory connectivity

To examine how pharmacological inhibition of GABA reuptake influences cortical GABA dynamics, we administered Tiagabine (Dalby, 2000; Chu et al., 2003)—a GAT-1 inhibitor—under 1% isoflurane anesthesia and measured extracellular GABA levels using iGABASnFR2. Before Tiagabine injection, visual stimulation evoked a robust and localized increase in GABA signals in the contralateral visual cortex (**Figure 6Ai**). Following Tiagabine administration, however, the same sensory stimulus failed to evoke a comparable response, with the activation map showing minimal or no detectable increase (**Figure 6Aii**). This reduction in evoked response is also reflected in the averaged traces (**Figure 6Aiii**), where the post-injection GABA response is blunted despite an overall upward shift in the baseline signal. To clarify this apparent paradox, we analyzed the raw fluorescence signal over time (**Figure 6Bi**). Tiagabine induced a sustained elevation in baseline iGABASnFR2 fluorescence, consistent with increased extracellular GABA resulting from GAT-1 blockade. Despite this elevation, the diminished responsiveness to stimulation suggests that high ambient GABA levels may saturate the sensor or reduce the responsiveness of inhibitory circuits. Quantification across multiple cortical areas confirmed a significant increase in baseline GABA levels (**Figure 6Bii**), and the spatial layout of analyzed ROIs is shown in (**Figure 6Biii**). We next investigated how this global increase in GABA levels influenced cortical connectivity. Seed-pixel correlation analysis (0.1–5 Hz) revealed reorganized correlation patterns following Tiagabine injection (**Figure 6Biv**). Seed regions in sensory cortices—barrel, forelimb, hindlimb, and visual—showed stronger local synchrony and broader spatial spread of GABA signal correlations. In addition, interhemispheric correlation matrices revealed increased bilateral connectivity post-Tiagabine (**Figure 6Bv**), suggesting enhanced cortical coordination during anesthesia. **Supplementary Figure 6** further supports these findings, showing increased low-

frequency (<1 Hz) oscillatory power and greater temporal modulation of the global signal after injection. Together, these results demonstrate that GAT-1 inhibition under anesthesia elevates extracellular GABA and reshapes large-scale cortical connectivity. While sensory-evoked GABA responses are suppressed—possibly due to sensor saturation or reduced network responsiveness—spontaneous activity becomes more spatially and temporally synchronized. These results further validate the ability of iGABASnFR2 to detect changes in extracellular GABA levels under both baseline and stimulated conditions, highlighting its sensitivity to dynamic alterations in cortical inhibition and its potential utility in pharmacological studies targeting GABAergic signaling.

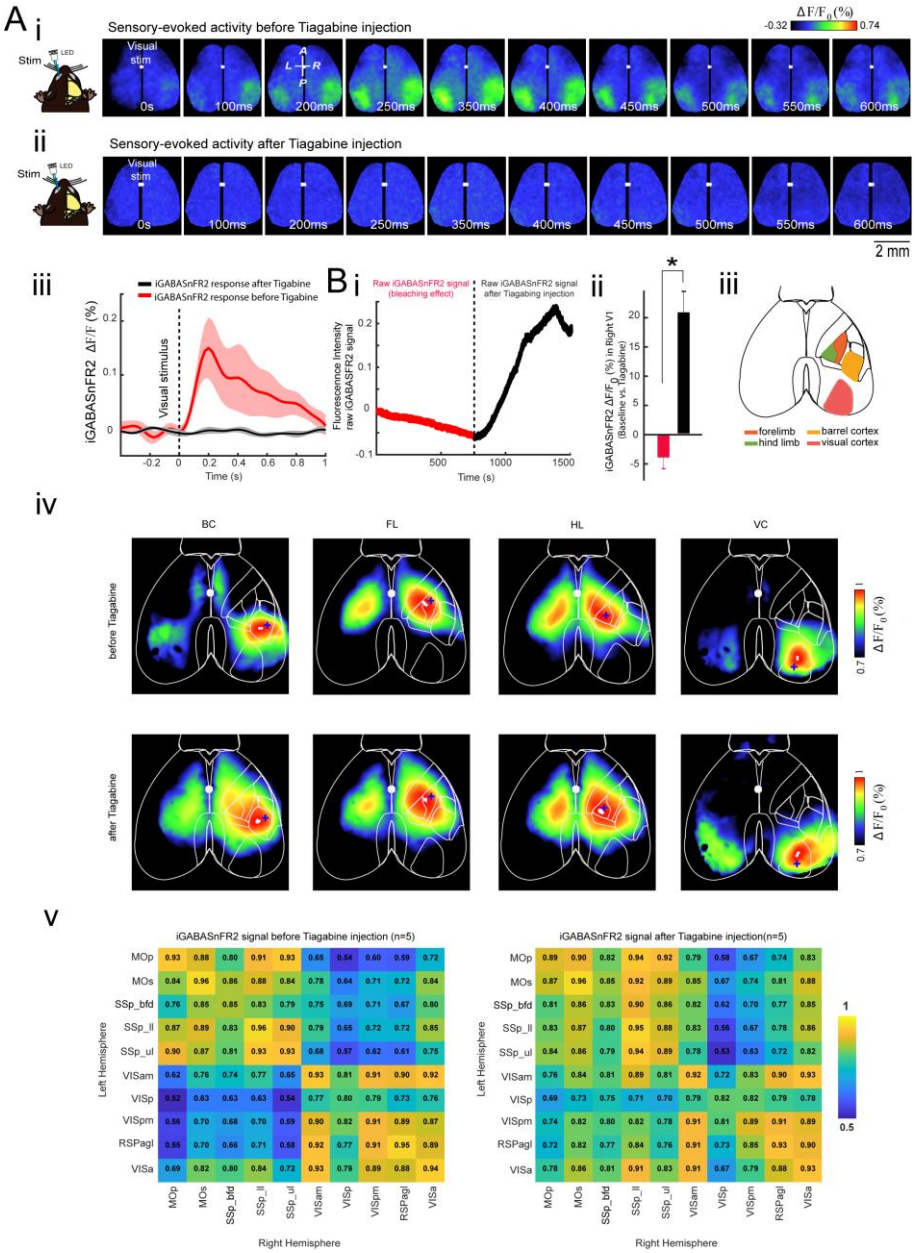

581 **Figure 6. Effect of Tiagabine administration on extracellular GABA activity in mice**
582 **expressing iGABASnFR2.** (A) Sensory-evoked GABA responses before and after Tiagabine
583 injection. (i) Representative montages of GABAergic activity evoked by visual stimulation before
584 Tiagabine administration. (ii) The same stimulation after Tiagabine injection. (iii) Time series of
585 contralateral visually evoked GABA responses before (red) and after (black) Tiagabine injection.
586 Data are presented as mean ± SEM, with responses extracted from 3 × 3-pixel regions of interest
587 (ROI) (~0.04 mm^2), n =5. (B) Tiagabine-induced changes in spontaneous GABA activity and
588 functional connectivity. (i) Raw fluorescence traces of iGABASnFR2 signal before (red) and after
589 (black) Tiagabine injection. The downward trend in the red trace reflects photobleaching (ii)
590 Quantification of GABA fluorescence change across cortical regions before and after Tiagabine
591 injection. Data represent mean ± SEM;paired *t*-test. ($P < 0.05$). (iii) Illustration of cortical regions
592 of interest (ROIs) used for seed-pixel correlation analysis. (iv) Seed-pixel correlation maps (0.1–
593 5 Hz) of spontaneous iGABASnFR2 activity before and after Tiagabine injection. Blue asterisks
594 indicate seed locations. (v) Interhemispheric correlation matrices before and after Tiagabine
595 injection. Regions: MOp – Primary motor area, MOs – Secondary motor area, SSp_bfd – Primary
596 somatosensory area (barrel field), SSp_ll – Lower limb, SSp_ul – Upper limb, VISam –
597 Anteromedial visual area, VISp – Primary visual area, VISpm – Posteromedial visual area, RSPagl
598 – Agranular retrosplenial area, VISa – Anterior visual area. The interior is at the top of all maps.
599 Blue crosses indicate the location of the seed pixel used for correlation mapping.

600 **Discussion**

601 We used mesoscale imaging with the genetically encoded GABA sensor iGABASnFR2 to map
602 the spatiotemporal dynamics of **extracellular GABA** across the intact mouse cortex in vivo. By
603 characterizing both sensory-evoked and spontaneous changes in extracellular GABA across
604 distinct brain states—including anesthesia, quiet wakefulness, NREM, and REM sleep—we
605 provide, for the first time, a comprehensive mesoscale view of GABA dynamics in the mammalian
606 brain. These findings establish iGABASnFR2 as a valuable tool for investigating GABAergic tone
607 and state-dependent fluctuations in extracellular GABA, complementing previous studies that used
608 iGluSnFR and voltage-sensitive dyes to map excitatory signaling and depolarization across large-
609 scale cortical networks (Mohajerani et al., 2013; Xie et al., 2016). The robust and state-dependent
610 changes in extracellular GABA we observed—during sensory stimulation, spontaneous activity,
611 and pharmacological manipulation—demonstrate that inhibitory tone is dynamically regulated
612 across brain states and cortical regions.

613 **Interpreting iGABASnFR2 signals**

614 iGABASnFR2 fluorescence changes are likely shaped by a combination of GABA release from
615 interneurons, diffusion through the extracellular space, and clearance by GABA transporters,
616 particularly GAT-1 (Scimemi, 2014; Overstreet & Westbrook, 2003; Glykys & Mody, 2007). The
617 temporal profile of sensory-evoked responses—characterized by a delayed onset (~75 ms) and

618 prolonged signal lasting several hundred milliseconds—is consistent with the dynamics of SST-
619 positive interneuron-mediated inhibition, which is known to follow the rapid activation of PV+
620 interneurons (Gabernet et al., 2005; Muñoz et al., 2017). The extended decay of iGABASnFR2
621 signals (**Figure 2C**) suggests that extracellular GABA may persist longer than typically assumed,
622 potentially contributing to modulatory or volume transmission effects.

623 Our pharmacological experiments with Tiagabine (**Figure 6Bi**) further support this interpretation,
624 demonstrating that GABA transporter activity plays a key role in shaping the extracellular GABA
625 signal detected by iGABASnFR2. Tiagabine administration led to a sustained increase in baseline
626 fluorescence (**Figure 6Bi**), consistent with reduced GABA clearance, and a concurrent reduction
627 in stimulus-related signal changes (**Figure 6Aiii**). This pattern suggests that elevated ambient
628 GABA may limit the detectability of stimulus-associated transients, possibly due to partial sensor
629 saturation or reduced dynamic range under high extracellular GABA conditions. Similar findings
630 have been reported with iGluSnFR, where glutamate transporter blockade enhanced baseline
631 signal without substantially altering response kinetics under some in vivo conditions (Xie et al.,
632 2016). In our case, the Tiagabine-induced increase in iGABASnFR2 signal highlights the sensor's
633 ability to detect pharmacologically induced changes in GABA levels and confirms its sensitivity
634 to shifts in extracellular GABA tone (**Supplementary Figure 6**).

635 **Cortical GABA responses to sensory input are conserved across brain states**

636 Our sensory-evoked experiments revealed consistent, modality-specific patterns of extracellular
637 GABA activation across the cortex, reflecting both localized responses and broader, network-level
638 dynamics (**Figure 2A**). Each stimulus modality selectively activated its corresponding primary
639 sensory area (**Figure 2B**), with activity spreading from the focal point of stimulation to more distal,
640 functionally connected cortical regions (**Figure 2A**). This widespread response pattern suggests
641 that inhibitory activity—like depolarizing signals observed in VSD imaging studies (Ferezou et
642 al., 2007; Mohajerani et al., 2013)—can propagate across large-scale networks, challenging the
643 traditional view of inhibition as strictly local. Our findings support the idea that extracellular
644 GABA dynamics reflect coordinated cortical processing, contributing to global inhibitory
645 regulation rather than isolated, local modulation (**Supplementary Figure 4**).

646 Contralateral responses were consistently stronger and faster than ipsilateral responses, likely due
647 to direct thalamocortical input, whereas delayed and weaker ipsilateral responses are consistent
648 with slower callosal transmission and interhemispheric integration (**Figure 2B–C**). These lateral

649 differences in timing and amplitude parallel those observed in iGluSnFR and VSD studies and
650 highlight known hemispheric asymmetries in signal propagation and network coordination (Xie et
651 al., 2016; Mohajerani et al., 2013). Importantly, these sensory-evoked GABA responses were
652 preserved across quiet wakefulness and anesthesia (**Figure 3B–D**). Despite differences in global
653 cortical state and arousal, the spatial and temporal patterns of GABA activation remained stable,
654 suggesting that sensory-driven inhibitory responses maintain functional consistency across brain
655 states. This robustness underscores the reliability of iGABASnFR2 for monitoring inhibitory
656 dynamics and reflects the essential role of inhibition in stabilizing excitation and regulating cortical
657 gain, as also supported by prior calcium imaging studies in awake animals (Pakan et al., 2016).

658 **Spontaneous GABA dynamics reveal state-dependent connectivity**

659 We extended our analysis to spontaneous activity across natural sleep-wake cycles using
660 hippocampal LFP and EMG for behavioral classification (**Figure 4A–C**). During quiet
661 wakefulness and NREM sleep, we observed robust bilateral and long-range synchronization of
662 GABA signals, forming reproducible functional connectivity maps (**Figures 4F–G, 5A–B**). In
663 contrast, REM sleep was characterized by reduced GABA amplitude, decreased low-frequency
664 fluctuations, and diminished interhemispheric correlations (**Figures 4D–E, 4G, 5Biii**). These
665 findings suggest that GABAergic network and its functional integration are dynamically
666 modulated by behavioral state. During NREM, widespread GABA synchrony likely reflects slow-
667 wave oscillations (**Figure 4E**), similar to excitatory activity patterns observed with iGluSnFR
668 (Karimi Abadchi et al., 2020). In REM, the cortex enters a desynchronized, activated state where
669 inhibition is relatively disengaged. The observation of rapid re-engagement of cortical GABA
670 during REM-to-wake transitions (**Figures 4H–I**) provides compelling evidence for the active role
671 of inhibition in re-stabilizing networks and reconfiguring circuits for sensory engagement upon
672 arousal.
673
674

675 **Functional inhibitory architecture aligns with cortical structural organization**

676 Seed-pixel correlation maps generated from iGABASnFR2 data revealed structured long-range
677 inhibitory connectivity that reflects known anatomical pathways (**Figure 5A**). In the awake state,
678 we observed high bilateral synchrony between homologous sensory areas and strong local

correlations within modalities (**Figure 5Ai, 5Bi**). These maps closely resemble those derived from excitatory indicators, including iGluSnFR and VSD (Xie et al., 2016; Mohajerani et al.,2013; Mohajerani et al.,2010), reinforcing the notion that both excitatory and inhibitory dynamics are scaffolded by the same structural connections. During NREM sleep, long-range inhibitory connectivity weakened, while local synchrony persisted, suggesting a shift toward localized processing and reduced cross-regional coordination (**Figures 5Aii, 5Bii)**. REM sleep partially restored these connections, albeit with diminished strength (**Figures 5Aiii, 5Biii**). These state-dependent changes highlight the flexibility of cortical inhibitory organization, which appears to adapt dynamically to behavioral state—promoting broad coordination during wakefulness and preserving localized stability during sleep.

Tiagabine modulates extracellular GABA and reorganizes cortical synchrony

Under isoflurane anesthesia, we administered Tiagabine to inhibit GABA reuptake and assess the role of transporter-mediated clearance in shaping extracellular GABA dynamics (Figure 6Bi; Supplementary Figure 6). Tiagabine led to a sustained elevation in baseline iGABASnFR2 fluorescence, consistent with increased extracellular GABA concentrations (Figure 6Bi). Notably, sensory-evoked responses were markedly reduced following Tiagabine injection (Figure 6Aiii), suggesting that elevated baseline GABA may constrain stimulus-driven increases, potentially due to sensor saturation or reduced responsiveness of GABA dynamics. In parallel, Tiagabine enhanced the spatial extent and strength of interhemispheric correlations in spontaneous GABA activity, indicating a reorganization of cortical inhibitory network dynamics and increased mesoscale synchrony (Figures 6Biv–v). These findings highlight the importance of GABA transporters in regulating extracellular GABA levels and shaping cortical coordination, even under anesthetized conditions. Furthermore, we demonstrate that iGABASnFR2 effectively captures both spontaneous and pharmacologically induced shifts in extracellular GABA, underscoring its value for probing inhibitory dynamics in both baseline and perturbed cortical states.

Conclusion

Together, our results establish iGABASnFR2 as a powerful sensor for in vivo imaging of extracellular GABA with high temporal and spatial resolution. From robust, stimulus-locked responses to dynamic, state-dependent motifs of spontaneous activity, the GABAergic signals captured by iGABASnFR2 offer a novel perspective on cortical network function. These data reveal that inhibition is not merely reactive or local but rather organized into large-scale motifs

that shift with behavioral state and can be tuned pharmacologically. Future work combining iGABASnFR2 with indicators of excitatory activity (e.g., iGluSnFR or calcium sensors) and with optogenetic control of interneuron subtypes will further dissect the interactions between excitation and inhibition across brain states. Moreover, using sparse expression and two-photon imaging could reveal how these mesoscale patterns arise from coordinated cellular ensembles. Finally, the ability to monitor GABAergic tone across sleep, wakefulness, and pharmacological interventions opens new avenues for studying diseases marked by inhibitory dysfunction, including epilepsy, schizophrenia, and neurodevelopmental disorders. By providing a direct readout of extracellular GABA, iGABASnFR2 serves as a critical bridge between cellular-level inhibition and systems-level dynamics.

Acknowledgments

We thank Di Shao and the Animal Welfare Committee at the University of Lethbridge for their support in enabling the animal experiments. We also thank Majid H. Mohajerani for providing access to laboratory resources and equipment during the data collection phase of this project.

Funding

The author(s) declare that financial support was received for the research, authorship, and/or publication of this article. This work was supported by Alberta Innovate and Natural Sciences and Engineering Research Council of Canada (grant 390930), awarded to Majid H. Mohajerani.

Author contributions

N.M. and T.H.M. performed the initial experiments. E.R. conceptualized the study. E.R. designed and conducted the main experiments. M.N. contributed to additional experimental procedures. J.K.A. implemented the strobing imaging system. E.R. and S.T. analyzed the data. E.R. prepared all the figures and wrote the manuscript. All authors have read and agreed to the submitted version of the manuscript.

Supplementary material

735 Supplementary material and methods are available.

736 **Disclosures**

737 The authors declare that there are no financial interests, commercial affiliations, or other potential
738 conflicts of interest that could have influenced the objectivity of this research or the writing of this
739 paper.

740 **The code and data Availability**

741 The code and all data analyzed and used to produce the main findings of this study have been
742 deposited on Dryad. Source data files are available for Figures 2, 3, 5, and 6.

743 **References**

744

745 Zhou, Y., & Danbolt, N. C. (2014). Glutamate as a neurotransmitter in the healthy brain. *Journal*
746 *of Neural Transmission*, *121*(8), 799–817. https://doi.org/10.1007/s00702-014-1180-8
747 Froemke, R. C. (2015). Plasticity of cortical excitatory-inhibitory balance. *Annual Review of*
748 *Neuroscience*, *38*, 195–219. https://doi.org/10.1146/annurev-neuro-071714-034002
749 Tatti, R., Haley, M. S., Swanson, O. K., Tselha, T., & Maffei, A. (2017). Neurophysiology and
750 regulation of the balance between excitation and inhibition in neocortical circuits. *Biological*
751 *Psychiatry, 81*(10), 821–831. https://doi.org/10.1016/j.biopsych.2016.09.017
752 Yuste, R. (2005). Origin and classification of neocortical interneurons. *Neuron, 48*(4), 524–527.
753 https://doi.org/10.1016/j.neuron.2005.11.012
754 Markram, H., Toledo-Rodriguez, M., Wang, Y., Gupta, A., Silberberg, G., & Wu, C. (2004).
755 Interneurons of the neocortical inhibitory system. *Nature Reviews Neuroscience, 5*(10), 793–807.
756 https://doi.org/10.1038/nrn1519
757 Tremblay, R., Lee, S., & Rudy, B. (2016). GABAergic interneurons in the neocortex: From
758 cellular properties to circuits. *Neuron, 91*(2), 260–292.
759 https://doi.org/10.1016/j.neuron.2016.06.033

Kepecs, A., & Fishell, G. (2014). Interneuron cell types are fit to function. *Nature, 505*(7483), 318–326. https://doi.org/10.1038/nature12983

Ferguson, B. R., & Gao, W.-J. (2018). PV interneurons: Critical regulators of E/I balance for prefrontal cortex-dependent behavior and psychiatric disorders. *Frontiers in Neural Circuits, 12*, Article 37. https://doi.org/10.3389/fncir.2018.00037

Urban-Ciecko, J., & Barth, A. L. (2016). Somatostatin-expressing neurons in cortical networks. *Nature Reviews Neuroscience, 17*(7), 401–409. https://doi.org/10.1038/nrn.2016.53

De Lanerolle, N. C., Kim, J. H., Robbins, R. J., & Spencer, D. D. (1989). Hippocampal interneuron loss and plasticity in human temporal lobe epilepsy. *Brain Research, 495*(2), 387–395. https://doi.org/10.1016/0006-8993(89)90234-5

Lewis, D. A., & Moghaddam, B. (2006). Cognitive dysfunction in schizophrenia: Convergence of γ-aminobutyric acid and glutamate alterations. *Archives of Neurology, 63*(10), 1372–1376. https://doi.org/10.1001/archneur.63.10.1372

Curley, A. A., & Lewis, D. A. (2012). Cortical basket cell dysfunction in schizophrenia. *The Journal of Physiology, 590*(Pt 4), 715–724. https://doi.org/10.1113/jphysiol.2011.224659

Marín, O. (2012). Interneuron dysfunction in psychiatric disorders. *Nature Reviews Neuroscience, 13*(2), 107–120. https://doi.org/10.1038/nrn3155

Rubenstein, J. L. R., & Merzenich, M. M. (2003). Model of autism: Increased ratio of excitation/inhibition in key neural systems. *Genes, Brain and Behavior, 2*(5), 255–267. https://doi.org/10.1034/j.1601-183x.2003.00037.x

Ben-Ari, Y. (2006). Seizures beget seizures: The quest for GABA as a key player. *Critical Reviews in Neurobiology, 18*(1–2), 135–144. https://doi.org/10.1615/critrevneurobiol.v18.i1-2.140

Gonzalez-Burgos, G., & Lewis, D. A. (2008). GABA neurons and the mechanisms of network oscillations: Implications for understanding cortical dysfunction in schizophrenia. *Schizophrenia Bulletin, 34*(5), 944–961. https://doi.org/10.1093/schbul/sbn070

Marvin, J. S., Borghuis, B. G., Tian, L., Cichon, J., Harnett, M. T., Akerboom, J., Gordus, A., Renninger, S. L., Chen, T.-W., Bargmann, C. I., Orger, M. B., Schreiter, E. R., Demb, J. B., Gan, W.-B., Hires, S. A., & Looger, L. L. (2013). An optimized fluorescent probe for visualizing glutamate neurotransmission. *Nature Methods, 10*(2), 162–170. https://doi.org/10.1038/nmeth.2333

Marvin, J. S., Scholl, B., Wilson, D. E., Podgorski, K., Kazemipour, A., Müller, J. A., Schoch, S., Urra Quiroz, F. J., Rebola, N., Bao, H., Little, J. P., Tkachuk, A. N., Cai, E., Hantman, A. W., Wang, S. S.-H., DePiero, V. J., Borghuis, B. G., Chapman, E. R., Dietrich, D., DiGregorio, D. A., Fitzpatrick, D., & Looger, L. L. (2018). Stability, affinity, and chromatic variants of the glutamate sensor iGluSnFR. *Nature Methods, 15*(11), 936–939. https://doi.org/10.1038/s41592-018-0171-3

Xie, Y., Chan, A. W., McGirr, A., Xue, S., Xiao, D., Zeng, H., & Murphy, T. H. (2016). Resolution of high-frequency mesoscale intracortical maps using the genetically encoded glutamate sensor iGluSnFR. *The Journal of Neuroscience, 36*(4), 1261–1272. https://doi.org/10.1523/JNEUROSCI.2744-15.2016

Marvin, J. S., Shimoda, Y., Magloire, V., Leite, M., Kawashima, T., Jensen, T. P., Kolb, I., Knott, E. L., Novak, O., Podgorski, K., Leidenheimer, N. J., Rusakov, D. A., Ahrens, M. B., Kullmann, D. M., & Looger, L. L. (2019). A genetically encoded fluorescent sensor for in vivo imaging of GABA. *Nature Methods, 16*(8), 763–770. https://doi.org/10.1038/s41592-019-0471-2

Yardeni, T., Eckhaus, M., Morris, H. D., Huizing, M., & Hoogstraten-Miller, S. (2011). Retro-orbital injections in mice. *Lab Animal, 40*(5), 155–160. https://doi.org/10.1038/laban0511-155

Chan, K. Y., Jang, M. J., Yoo, B. B., Greenbaum, A., Ravi, N., Wu, W.-L., Sánchez-Guardado, L., Lois, C., Mazmanian, S. K., Deverman, B. E., & Gradinaru, V. (2017). Engineered AAVs for efficient noninvasive gene delivery to the central and peripheral nervous systems. *Nature Neuroscience, 20*(8), 1172–1179. https://doi.org/10.1038/nn.4593

Vanni, M. P., & Murphy, T. H. (2014). Mesoscale transcranial spontaneous activity mapping in GCaMP3 transgenic mice reveals extensive reciprocal connections between areas of somatomotor cortex. *Journal of Neuroscience, 34*(48), 15931–15946. https://doi.org/10.1523/JNEUROSCI.1818-14.2014

Silasi, G., Xiao, D., Vanni, M. P., Chen, A. C. N., & Murphy, T. H. (2016). Intact skull chronic windows for mesoscopic wide-field imaging in awake mice. *Journal of Neuroscience Methods, 267*, 141–149. https://doi.org/10.1016/j.jneumeth.2016.04.012

Xiao, D., Forys, B. J., Vanni, M. P., & Murphy, T. H. (2021). MesoNet allows automated scaling and segmentation of mouse mesoscale cortical maps using machine learning. *Nature Communications, 12*(1), 5992. https://doi.org/10.1038/s41467-021-26255-2

Mohajerani, M. H., Chan, A. W., Mohsenvand, M., LeDue, J., Liu, R., McVea, D. A., Boyd, J. D., Wang, Y. T., Reimers, M., & Murphy, T. H. (2013). Spontaneous cortical activity alternates

between motifs defined by regional axonal projections. *Nature Neuroscience, 16*(10), 1426–1435. https://doi.org/10.1038/nn.3499

Afrashteh, N., Inayat, S., Bermudez-Contreras, E., Luczak, A., McNaughton, B. L., & Mohajerani, M. H. (2021). Spatiotemporal structure of sensory-evoked and spontaneous activity revealed by mesoscale imaging in anesthetized and awake mice. *Cell Reports, 37*(10), 110081. https://doi.org/10.1016/j.celrep.2021.110081

Yüzgeç, Ö., Prsa, M., Zimmermann, R., & Huber, D. (2018). Pupil size coupling to cortical states protects the stability of deep sleep via parasympathetic modulation. *Current Biology, 28*(3), 392–400.e3. https://doi.org/10.1016/j.cub.2017.12.049

Chen, Q., Cichon, J., Wang, W., Qiu, L., Lee, S.-J. R., Campbell, N. R., Destefino, N., Goard, M. J., Fu, Z., Yasuda, R., Looger, L. L., Arenkiel, B. R., Gan, W.-B., & Feng, G. (2012). Imaging neural activity using Thy1-GCaMP transgenic mice. *Neuron, 76*(2), 297–308. https://doi.org/10.1016/j.neuron.2012.07.011

Atallah, B. V., Bruns, W., Carandini, M., & Scanziani, M. (2012). Parvalbumin-expressing interneurons linearly transform cortical responses to visual stimuli. *Neuron, 73*(1), 159–170. https://doi.org/10.1016/j.neuron.2011.12.013

Wilson, N. R., Runyan, C. A., Wang, F. L., & Sur, M. (2012). Division and subtraction by distinct cortical inhibitory networks in vivo. *Nature, 488*, 343–348. https://doi.org/10.1038/nature11347

Petersen, C. C. H. (2007). The functional organization of the barrel cortex. *Neuron*, 56(2), 339–355. https://doi.org/10.1016/j.neuron.2007.09.017

Ridder, W. H., & Nusinowitz, S. (2006). The visual evoked potential in the mouse—Origins and response characteristics. *Vision Research*, 46(6–7), 902–913. https://doi.org/10.1016/j.visres.2005.09.006

Gabernet, L., Jadhav, S. P., Feldman, D. E., Carandini, M., & Scanziani, M. (2005). Somatosensory integration controlled by dynamic thalamocortical feed-forward inhibition. *Neuron*, 48(2), 315–327. https://doi.org/10.1016/j.neuron.2005.09.022

Isaacson, J. S., & Scanziani, M. (2011). How inhibition shapes cortical activity. *Neuron*, 72(2), 231–243. https://doi.org/10.1016/j.neuron.2011.09.027

Muñoz, W., Tremblay, R., Levenstein, D., & Rudy, B. (2017). Layer-specific modulation of neocortical dendritic inhibition during active wakefulness. *Science*, 355(6328), 954–959. https://doi.org/10.1126/science.aag2599

Gentet, L. J., Kremer, Y., Taniguchi, H., Huang, Z. J., & Petersen, C. C. H. (2012). Unique functional properties of somatostatin-expressing GABAergic neurons in mouse barrel cortex. *Nature Neuroscience*, 15(4), 607–612. https://doi.org/10.1038/nn.3051

Urban-Ciecko, J., & Barth, A. L. (2016). Somatostatin-expressing neurons in cortical networks. *Nature Reviews Neuroscience*, 17(7), 401–409. https://doi.org/10.1038/nrn.2016.53

Ferezou, I., Haiss, F., Gentet, L. J., Aronoff, R., Weber, B., & Petersen, C. C. H. (2007). Spatiotemporal dynamics of cortical sensorimotor integration in behaving mice. *Neuron*, 56(5), 907–923. https://doi.org/10.1016/j.neuron.2007.10.007

Minamisawa, G., Kwon, S. E., Chevee, M., Brown, S. P., & O'Connor, D. H. (2018). A non-canonical feedback circuit for rapid interactions between somatosensory cortices. *Cell Reports*, 23(9), 2718–2731. https://doi.org/10.1016/j.celrep.2018.04.113

Pakan, J. M. P., Currie, S. P., Fischer, L., & Rochefort, N. L. (2018). The impact of visual cues, reward, and motor feedback on the representation of behaviorally relevant spatial locations in primary visual cortex. *Cell Reports, 24*(10), 2521–2528. https://doi.org/10.1016/j.celrep.2018.08.010

Gentet, L. J., Avermann, M., Matyas, F., Staiger, J. F., & Petersen, C. C. H. (2010). Membrane potential dynamics of GABAergic neurons in the barrel cortex of behaving mice. *Neuron, 65*(3), 422–435. https://doi.org/10.1016/j.neuron.2010.01.006

Pakan, J. M. P., Lowe, S. C., Dylda, E., Keemink, S. W., Currie, S. P., Coutts, C. A., & Rochefort, N. L. (2016). Behavioral-state modulation of inhibition is context-dependent and cell type specific in mouse visual cortex. *eLife, 5*, e14985. https://doi.org/10.7554/eLife.14985

Keller, G. B., & Mrsic-Flogel, T. D. (2018). Predictive processing: A canonical cortical computation. *Neuron, 100*(2), 424–435. https://doi.org/10.1016/j.neuron.2018.10.003

McGinley, M. J., Vinck, M., Reimer, J., Batista-Brito, R., Zagha, E., Cadwell, C. R., Tolias, A. S., Cardin, J. A., & McCormick, D. A. (2015). Waking state: Rapid variations modulate neural and behavioral responses. *Neuron, 87*(6), 1143–1161. https://doi.org/10.1016/j.neuron.2015.09.012

Pfeffer, C. K., Xue, M., He, M., Huang, Z. J., & Scanziani, M. (2013). Inhibition of inhibition in visual cortex: The logic of connections between molecularly distinct interneurons. *Nature Neuroscience, 16*(8), 1068–1076. https://doi.org/10.1038/nn.3446

Dash, M. B., Douglas, C. L., Vyazovskiy, V. V., Cirelli, C., & Tononi, G. (2009). Long-term homeostasis of extracellular glutamate in the rat cerebral cortex across sleep and waking states. *Journal of Neuroscience, 29*(3), 620–629. https://doi.org/10.1523/JNEUROSCI.5486-08.2009

Karimi Abadchi, J., Nazari-Ahangarkolaee, M., Gattas, S., Bermudez-Contreras, E., Luczak, A., McNaughton, B. L., & Mohajerani, M. H. (2020). Spatiotemporal patterns of neocortical activity around hippocampal sharp-wave ripples. *eLife, 9*, e51972. https://doi.org/10.7554/eLife.51972

Nazari, M., Karimi Abadchi, J., Naghizadeh, M., Bermudez-Contreras, E. J., McNaughton, B. L., Tatsuno, M., & Mohajerani, M. H. (2023). Regional variation in cholinergic terminal activity determines the non-uniform occurrence of cortical slow waves during REM sleep in mice. *Cell Reports, 42*(5), 112450. https://doi.org/10.1016/j.celrep.2023.112450

Karimi Abadchi, J., Rezaei, Z., Knöpfel, T., McNaughton, B. L., & Mohajerani, M. H. (2023). Inhibition is a prevalent mode of activity in the neocortex around awake hippocampal ripples in mice. *eLife, 12*, e79513. https://doi.org/10.7554/eLife.79513

Rynes, M. L., Surinach, D. A., Linn, S., Laroque, M., Rajendran, V., Dominguez, J., Hadjistamoulou, O., Navabi, Z. S., Ghanbari, L., Johnson, G. W., Nazari, M., Mohajerani, M. H., & Kodandaramaiah, S. B. (2021). Miniaturized head-mounted microscope for whole-cortex mesoscale imaging in freely behaving mice. *Nature Methods, 18*(4), 417–425. https://doi.org/10.1038/s41592-021-01104-8

Wu, Y., Wang, W., & Richerson, G. B. (2001). GABA transaminase inhibition induces spontaneous and enhances depolarization-evoked GABA efflux via reversal of the GABA transporter. *Journal of Neuroscience, 21*(8), 2630–2639. https://doi.org/10.1523/JNEUROSCI.21-08-02630.2001

Fink-Jensen, A., Suzdak, P. D., Swedberg, M. D., Judge, M. E., Hansen, L., & Nielsen, P. G. (1992). The gamma-aminobutyric acid (GABA) uptake inhibitor, tiagabine, increases extracellular brain levels of GABA in awake rats. *European Journal of Pharmacology, 220*(2–3), 197–201. https://doi.org/10.1016/0014-2999(92)90748-s

Scimemi, A. (2014). Plasticity of GABA transporters: An unconventional route to shape inhibitory synaptic transmission. *Frontiers in Cellular Neuroscience, 8*, 128. https://doi.org/10.3389/fncel.2014.00128

Overstreet, L. S., & Westbrook, G. L. (2003). Synapse density regulates independence at unitary inhibitory synapses. *Journal of Neuroscience, 23*(7), 2618–2626. https://doi.org/10.1523/JNEUROSCI.23-07-02618.2003

Glykys, J., & Mody, I. (2007). The main source of ambient GABA responsible for tonic inhibition in the mouse hippocampus. *The Journal of Physiology, 582*(Pt 3), 1163–1178. https://doi.org/10.1113/jphysiol.2007.134460

Mohajerani, M. H., McVea, D. A., Fingas, M., & Murphy, T. H. (2010). Mirrored bilateral slow-wave cortical activity within local circuits revealed by fast bihemispheric voltage-sensitive dye imaging in anesthetized and awake mice. *Journal of Neuroscience, 30*(10), 3745–3751. https://doi.org/10.1523/JNEUROSCI.4423-09.2010